Bailey Donaldson
OCN 665
Professor Kelvin Richards

Heat Flux Anomalies Associated with Mesoscale Eddies

1. Introduction:

Until recently, oceanic data was far and few between. Measurements were from ships or buoys and had ranges of several hundred kilometers. Regions outside of standard shipping routes were rarely sampled. With the advent of satellite technology, spatial and temporal resolutions of ocean and atmospheric data are smaller than ever. This allows us to study the atmospheric and oceanic interaction of mesoscale features (10 – 1000 km) (Chelton and Xie 2010). Here we study mesoscale eddies because they have proven to have an important role in ocean fluxes and dynamics (Wunsch, 1999). We hope to further confirm the coupling of mesoscale air-sea interactions (e.g. Chelton and Xie 2010).

Here we shall examine an important feature that links the atmosphere and ocean: turbulent heat fluxes. Turbulent latent and sensible heat fluxes are the primary processes by which the ocean releases heat to the atmosphere (Cayan, 1992). Heat fluxes depend on air-specific humidity, sea surface temperature (SST), and wind speed. Recent works revealed that mesoscale eddies create anomalies amongst these parameters (e.g., Chelton and Xie 2010; Hausmann and Czaja, 2012). However, until the paper by Villas Bôas et al. (2015), the signature of mesoscale eddies on these fluxes had not been sufficiently examined. This report will thoroughly examine the 2015 paper by Villas Bôas et al. titled "The signature of mesoscale eddies on the air-sea turbulent heat fluxes in the South Atlantic Ocean" to undercover the details behind their interaction and the methodology necessary to uncover it.

The Villas Bôas et al. (2015) paper utilizes latent heat flux (LHF) and sensible heat flux (SHF) calculations from the *French Institute for Exploitation of the Sea* (IFREMER) (Bentamy et al., 2013). The 2013 improvements made by IFREMER calculate the LHF and SHF on a 0.25º x 0.25º grid. This resolution is fine enough to expose mesoscale variability in surface heat fluxes. To identify eddies, satellite sea level anomaly (SLA) data and eddy identification methodology by Chaigneau et al. (2009) was used. The details of the LHF and SHF calculations as well as the eddy identification method will be explored below. Lastly, we will observe the impact of mesoscale ocean eddies on the LHF and SHF in the South Atlantic Ocean (SA).

2. Eddies:

2.1: Defining Eddies

Eddies are mesoscale vortices. They are generally more energetic than the surrounding currents. Their typical horizontal scale is 50-300km and their time scale is from weeks to months (Chelton et al., 2011). Eddies advect parcels of trapped fluid over time, which can significantly impact ocean dynamics and fluxes. Therefore, they are important for the large-scale transfer and redistribution of heat, salt, and momentum (Wunsch, C.,1999). Eddies exhibit anomalies of sea surface height, sea surface temperature (SST), and wind stress. Because they alter these things, they impact the air-sea fluxes and in turn, atmospheric circulation.
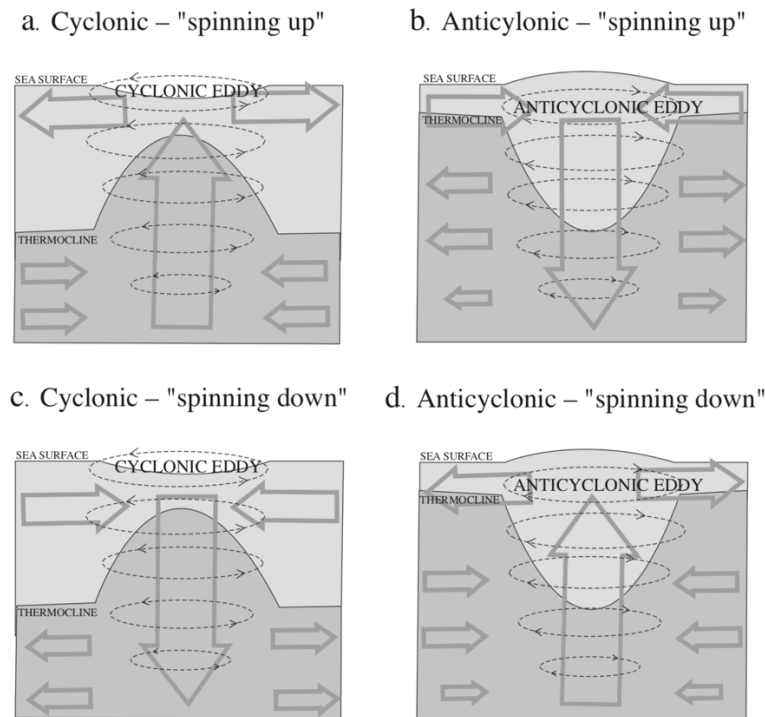
Figure 1: Vertical circulation patterns in (a) forced cyclonic eddy, (b) forced anticyclonic eddy, (c) a decaying free cyclonic eddy, (d) a decaying free anticyclonic eddy. (Source: Bakun 2006)

Eddies can be divided into cyclonic and anticyclonic eddies. Cyclonic eddies rotate around a low-pressure system and anticyclonic rotate around a high-pressure system. In the Southern Hemisphere, cyclonic eddies rotate clockwise and anticyclonic eddies rotate counterclockwise. They will have either a warm core or a cold core depending on if the eddies experience upwelling or downwelling. Most commonly, a cyclonic (anticyclonic) eddy will experience divergence (convergence) at the surface and convergence (divergence) in the interior, resulting in upwelling (downwelling) (Figure 1a, 1b). However, there are instances when the opposite is true (Figure 1c, 1d). The different scenarios are referred to as: "spinning up" vs. "spinning down" (Bakun, 2006). Eddies can also be expressed as either surface intensified or subsurface intensified, which is the terminology used in the Villas Bôas et al. (2015) paper. They depend on whether their core –or area where their potential vorticity reaches it maximum—is located inside the water column rather than in the surface layer. Distinguishing the two from one another is extremely challenging (Assassi et al., 2016). As a result, the heat flux anomalies as they differ (or agree) in surface intensified vs. subsurface intensified eddies is not studied here.

2.2: Eddy Identification

There are various methods for identifying eddies. Identification algorithms can be based on either physical or geometric criteria of the flow field. To identify eddies using physical criteria, one must make a calculation of dynamical properties, such as pressure, sea-level anomaly magnitude, high vorticity magnitude, or high normalized helicity. Then you would identify where thresholds of calculated properties are exceeded to find the eddies. However, these physical criteria are often inaccurate because they can fail to locate vortices. In addition,

this method does not require set thresholds, instead the user is required to participate in the eddy identification, resulting in a subjective process (Chaigneau, 2008).

The method of eddy identification based on the geometry of flow is more. The geometric criteria use the shape of instantaneous streamlines to detect eddies. It identifies vortices by examining a large number of streamlines over the velocity field and counting those that have circular or closed geometry. From here, eddies are identified by the "winding-angle" method, developed by Chaigneau et al. (2008). It was found to be more accurate than the curvature center method. The winding-angle method selects and clusters closed streamlines (see Fig 2). A streamline with a winding-angle higher than 2π is associated with an eddy (Chaigneau et al., 2008).
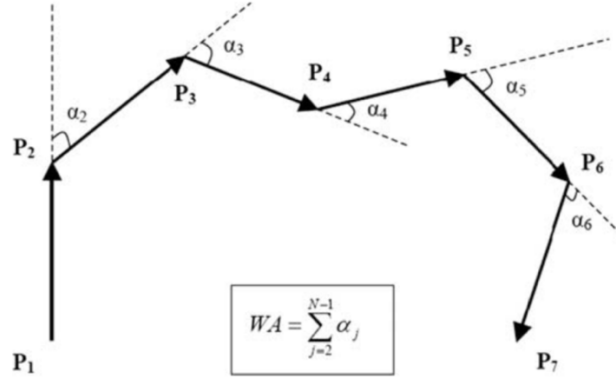

Figure 2: Winding-Angle schematic representation for a segmented streamline. (Source: Chaigneau 2008)

The Bôas et al. (2015) paper used a further developed version of the "winding-angle" method developed by Chaigneau et al. (2009) that utilized physical criteria of the flow field in addition to geometric criteria. The detection algorithm used first searches for eddy centers associated with sea-level anomaly (SLA) maxima and minima to find cyclonic and anticyclonic eddies, respectively. Then, around the maxima and minima, the algorithm searches for closed SLA contours. The edge of the eddy is identified by the outer closed SLA contour.

The eddy is tracked over its lifetime in 7-day increments by comparing each eddy at time t to those at time $t + \delta t$ (where $\delta t = 7$) within the radius of 150 km. A cost function is used to determine which eddies at t correspond to the eddies at $t + \delta t$. This is important because eddies may pass through gaps in satellite groundtracks and may not reappear for up to 3 weeks. The cost function compares eddies of the same polarity, cyclonic or anticyclonic. It depends on their distances, vortices, kinetic energy, and radii:

$$C_F = \left(\frac{\delta D}{50}\right)^2 + \left(\frac{\delta \xi}{1.3 \times 10^{-6}}\right)^2 + \left(\frac{\delta EKE}{10}\right)^2 + \left(\frac{\delta R}{10}\right)^2 \qquad (1)$$

The smaller the cost function, the more likely that the eddy at $t + \delta t$ is the same as the one at t. δD, $\delta \xi$, δEKE, and δR are the differences in distance, vorticity, eddy kinetic energy, and radius between the eddy at time t and all other eddies at time $t + \delta t$ (Chaigneau et al. (2009), Bôas et al. (2015)).

The Bôas et al. (2015) paper uses SLA data from the gridded multi-mission project by Ssalto/Ducas, distributed by Archiving, Validation, and Interpretation of Satellite Oceanographic data (AVISO) (http://www.aviso.oceanobs.com/duacs/). AVISO finds SLA data by defining it relative to a 7-year mean (1993-1999). It has a nominal precision of 2 cm and is distributed in a uniform ¼° grid at 7-day intervals. The time and spatial scales are small enough to detect mesoscale features, including eddies.

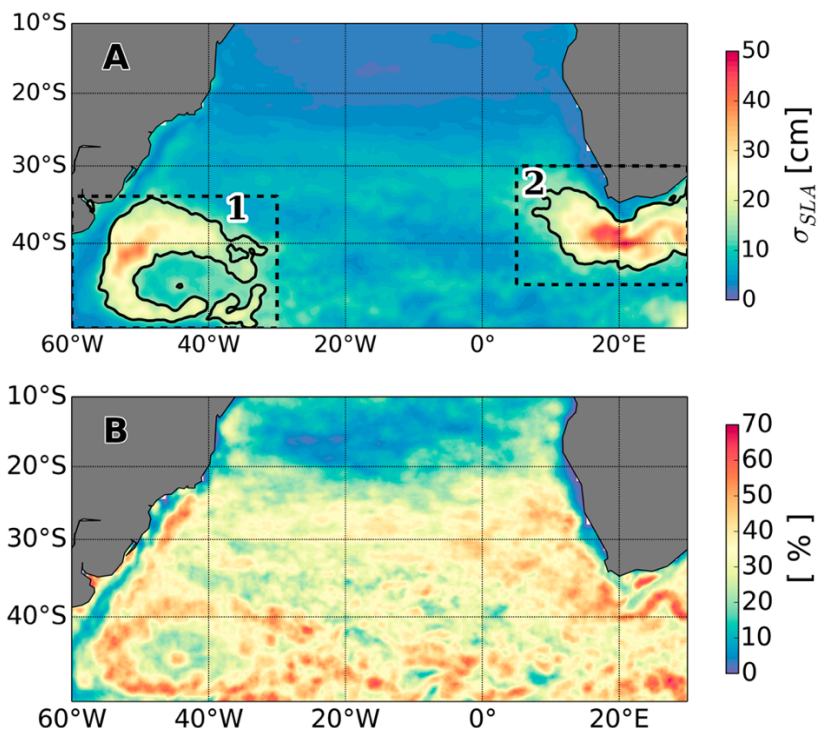*Figure 3: (a) The plot shows the standard deviation of the sea level anomaly (σ_{SLA}) over the entire time series (1999 – 2009). Regions with the largest values contain mesoscale features, including eddies, that have large amplitudes. The black solid contour is σ_{SLA} = 15 cm. Dashed box 1 encloses the Brazil-Malvinas confluence region (BMC) and dashed box 2 encloses the Agulhas Current Retroflection (AGR). (b) The plot shows the percentage of time that each grid point was inside an eddy during the entire time series (1999 – 2009), also known as the eddy frequency. (Source: Villas Bôas et al. 2015)*

Now that the eddies have been tracked and identified, we can observe their distribution over the region we will be working with (Fig 3). Villas Bôas et al. (2015) examines the South Atlantic. This region is ideal because it exhibits both an area of "calm" and two areas of energetic variability. The region with low eddy frequency is in the tropical South Atlantic between 10ºS and 20ºS where the eddy frequency ranges from 0 to 30%. Meanwhile, in the Brazil-Malvinas confluence region (BMC) and the Agulhas Current Retroflection (AGR), the eddy frequency reaches from 50% to 70% (Figure 3b). The typical range of eddy amplitude was between 2 cm and 50 cm, though eddy amplitude in the BCM and AGR regions were considerably larger; the eddy amplitude mode was ~5 cm. The mode of the eddy radius in the South Atlantic Ocean was 70 km, though typical radius varied from 30km to 175km (Fig 4).
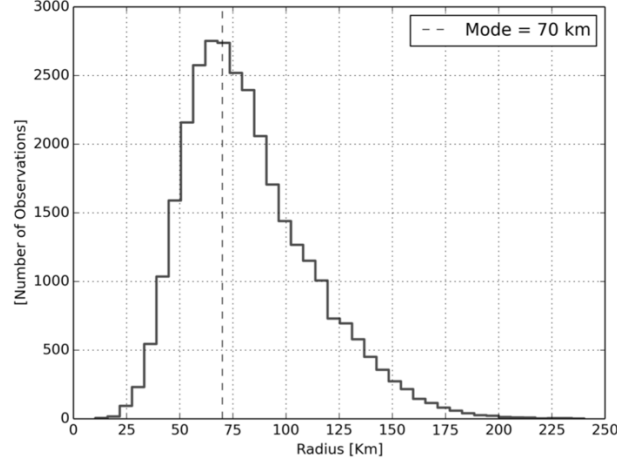
Figure 4: Histogram of the radius of all the eddies identified in the South Atlantic Ocean during the studied period (1999-2009). Mode is identified with the vertical dashed line. (Source: Villas Bôas et al., 2015)

3. Calculation of Turbulent Heat Fluxes

3.1: IFREMER Method

The calculations of the latent and sensible heat fluxes in the Villas Bôas et al. (2015) paper are based off of the daily satellite-based data from the *French Institute for Exploitation of the Sea* (IFREMER) (Bentamy et al. 2013). Their method estimates daily turbulent air-sea fluxes on a 0.25º grid across the global ocean. This resolution is sufficient to estimate LHF and SHF associated with mesoscale processes because most of the eddies analyzed have spatial scales of ~140 km (as discussed in Section 2.1). IFREMER provides daily LHF and SHF values from October 1999 to September 2009, which is sufficient time to study the heat flux influences on mesoscale eddies due to the "short" timescales of eddies (discussed in Section 2.1).

There are five variables required to estimate turbulent fluxes: wind speed (W_{10}), specific air humidity (Q_a), and air temperature (T_a), all of which are measured at 10 m altitude. We also require specific surface humidity (Q_s) and sea surface temperature (T_s or SST) at the sea surface (Bentamy et al. 2013, Santorelli et al. 2011). You can observe the use of these variables within LHF and SHF in the parameterization by Santorelli et al. (2011) below:

$$LHF = L_v \cdot \rho_a \cdot C_E \cdot W_{10} \cdot (Q_s - Q_a) \qquad (2a)$$

$$SHF = C_P \cdot \rho_a \cdot C_H \cdot W_{10}(T_s - T_a) \qquad (2b)$$

The constants are as follows: ρ_a is air density, L_v is latent heat of vaporization, C_p is the specific heat capacity of air at constant pressure, and C_E and C_H are moisture and heat exchange coefficients. Bentamy et al. (2013) finds the surface turbulent heat fluxes by combining the bulk algorithms of Fairall et al. (2003) with the five input parameters (W_{10}, Q_s, T_s, T_a, Q_a) explored below.

Table 1: Variables used to derive IFREMER Turbulent Heat Fluxes and their origin. All are listed except for Q_a, which is described in the text.

Variable	Source for IFREMER
Wind Speed (W_{10})	SeaWinds scatterometer onboard QuikSCAT, V3
Specific Surface Humidity (Q_s)	Assumed to be 98% of Q_a
Sea Surface Temperature (T_s)	V2 of IO daily analyses
Air Temperature (T_a)	ERA-Interm

       Satellite data is used to obtain the variables and they are corroborated with the use of moored buoys, ships, and NWP models. Wind is obtained from the SeaWinds scatterometer onboard the QuikSCAT satellite. QuikSCAT V3 data is used, which has been determined accurate by comparing it with buoy wind measurements, QuikSCAT V2 retrievals, and remotely sensed winds derived from the ASCAT scatterometer onboard Metop-A satellite (Bentamy et al. 2013). Specific surface humidity (Q_s) is assumed to be 98% of the saturation humidity at the sea surface temperature. Sea surface temperature (T_s) data is a version 2 of IO daily analyses (Reynolds et al., 2007) with a spatial resolution of 0.25º in longitude and latitude (Bentamy et al. 2013). Air temperature is obtained from the European Centre for Medium Range Weather Forecasts reanalysis (ERA—Interim) at 0.75º x 0.75º resolution. Of all the input variables used on the Bentamy et al. (2013) product, air temperature (T_a) has the lowest resolution. Bentamy et al. (2013) interpolates it onto a 0.25º x 0.25º grid, ensuring that the heat fluxes can be calculated on the smallest grid possible.

       Specific air humidity (Q_a) is the most challenging to retrieve. Many studies explored how to retrieve Q_a from brightness temperatures (e.g., Bentamy et al., 2003), but there is a need for an improved method of remotely sensed specific air humidity (Grodsky et al. (2009), Santorelli et al. (2011)). In past works, retrieving Q_a was based on the relationship between the microwave brightness temperatures (Tb) and Q_a which, in turn, is based on the quasi-linear relationship between Q_a and water vapor content (Schultz et al., 1993). The retrieval method used by IFREMER is a slight deviation from this method. The new Q_a retrieval method includes SST and the air-sea temperature difference term in addition to the traditional microwave brightness term. The Tb they use is measured by the Special Sensor Microwave Imager onboard the Defense Meteorological Satellite Program (DMSP) F11, F13, F14, and F15 satellites (SSM/I). To calibrate Q_a, SSM/I, the National Oceanography Centre Southampton Flux Dataset v2.0 (NOCS2.0), Era-Interim, and SST are collocated in space and time (Bentamy et al. 2013).

       After obtaining all five parameters, they calculate the LHF and SHF on the 0.25º x 0.25º grid. To check the accuracy of the calculations, they validate their findings against *in situ* data from buoys. In addition, they confirm their findings by using data of daily mean air-sea interaction from the NOCS2.0, which provides daily parameters such as W_{10}, Q_a, T_a, SST, LHF, and SHF, with uncertainty estimates. It is unclear why Bôas et al. (2009) decides to use the method created by Bentamy et al. (2013) instead of NOCS2.0 data.

3.2: Filtering

       Now that we understand how the LHF and SHF values are found, we look at how Villas Bôas et al. (2015) manipulates them to isolate the impact mesoscale eddies have on heat fluxes.

They are careful to include the cases when the surface turbulent heat fluxes are superimposed on large-scale features. The first step is to isolate mesoscale features by filtering LHF and SHF data in time and space. They apply a temporal band-pass Hann window to remove all periods outside of the range of periods from 7 to 90 days, which are the typical time scales of eddies. Then they remove the data from grid points located inside eddies from the time-filtered map. This gives them LHF and SHF maps of masked data, temporally filtered to remove periods that are not within eddy contours. Then they spatially low-pass filter these maps with an average Hann window of 600 km. Any signals that have wavelengths longer than 600 km are considered the large-scale reference. The large-scale reference level is subtracted from the time-filtered maps to get the LHF and SHF anomaly maps. The resulting LHF and SHF anomaly maps smooth out as much large-scale variability as possible yet retain the full variability of the eddies.

3.3: Composite Maps

Next, they created composite maps in order to observe the spatial patterns of the heat flux anomalies within the eddies and their immediate surroundings. For each identified eddy, LHF and SHF anomalies were interpolated onto a uniform high-resolution gird. The grid was normalized by the radial distance from the eddy center to the eddy edge. The maps display the anomaly field to a distance twice the eddy radius in each direction. This scaling allows one to average the anomaly of thousands of eddies as a single composite map (Villas Bôas et al. 2015). The composite maps were obtained by averaging eddies with the 5% highest absolute amplitudes ($\geq$ 27.3 cm), which corresponds to 4189 cyclonic and 4013 anticyclonic eddy realizations, and 1115 cyclonic and 979 anticyclonic individual eddies.
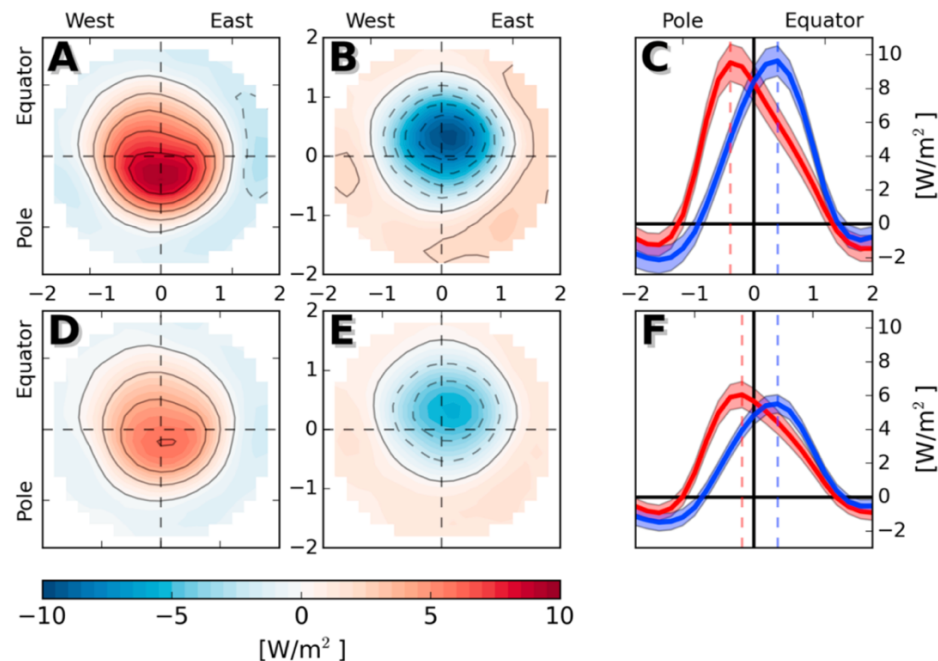

Figure 5: Averaged composite maps. (A) = LHF anomalies inside anticyclonic eddies; (B) = LHF anomalies inside cyclonic eddies; (D) = SHF anomalies inside anticyclonic eddies; E = SHF anomalies inside cyclonic eddies. The axis in the composite maps are the normalized distance between the eddy center and twice the eddy edge. Contour intervals are shown every 2 W/m². (C, F) = meridional section of the absolute values of

the LHF (C) and SHF (F) anomalies. Anticyclonic are red lines and cyclonic are blue lines. The shadow around the lines is one standard error of the mean. (Source: Villas Bôas et al. 2015)

4. Results and Discussion

It is well known that eddies have an imprint on SST, therefore one expects that they will also impact LHF and SHF, which are both dependent on temperature. As observed in Section 2.1, cold-core cyclonic eddies have negative SST anomalies, while warm-core anticyclonic eddies have positive SST anomalies (e.g., Fregner et al., 2013). As can be observed in the SHF equation 2b, SHF depends on the temperature gradient between the ocean and atmosphere. Therefore, a positive (negative) SST anomaly would increase (decrease) the temperature gradient, thereby increasing (decreasing) the SHF anomaly. LHF depends on the saturation humidity at the sea surface (Q_s) (Equation 2a). Saturation humidity is dependent on temperature because warm air is capable of containing more liquid. Therefore, if the amount of moisture in the air remains constant, an increase in temperature would result in a decrease in relative humidity. This is why it is expected that anticyclonic eddies contribute to positive heat flux anomalies (ocean heat loss), while cyclonic eddies contribute to negative anomalies (ocean heat gain).

In the composite maps, the peak of the LHF and SHF anomalies are of the $\pm 10 \pm 1$ W/m^2 and $\pm 6 \pm 0.6$ W/m^2 respectively (Fig 5). The LHF and SHF peak near, though not on, the center of the eddies and decrease radially outward, reaching minimum values near the eddy edge. The maximum anomalies are equatorward of the eddy center for cyclonic eddies and poleward for anticyclonic eddies. These meridional displacements occur for all eddy amplitude ranges, in addition to the ≥ 27.3 cm range shown Figure 5.

The off-center LHF and SHF anomaly peak is likely due to the beta (β) effect. Beta is the change of the Coriolis parameter (f) with latitude (ϕ).

$$\beta \equiv \frac{df}{dy} = \frac{2\Omega \cos \phi}{R} \qquad (4)$$

Mesoscale eddies are large enough that they experience the β-effect (Firing and Beardsley, 1976). f is larger at the poles and smaller near the equator. Therefore, as the ambient fluid parcels rotate with the eddy, f changes. Due to conservation of potential vorticity (PV) (Equation 6), relative vorticity (ζ) must change too.

$$PV = \frac{f + \zeta}{H} \qquad (5)$$

$$\frac{D}{Dt}\left(\frac{f + \zeta}{H}\right) = 0. \qquad (6)$$

As a result, cyclonic eddies in the Southern Hemisphere experience weak vorticity in the northern flank and strong vorticity in the southern flank. The resulting vorticity anomaly dipole induces upwelling in the northern flank and downwelling in the southern flank (anticyclonic eddies are the opposite). Cold core cyclonic eddies generally experience upwelling, which is the source of their cold core. But the addition of the dipole will result in the most upwelling, the coldest water, and the most negative heat flux anomalies, slightly north of the eddy center. The

opposite would occur for anticyclonic eddies, resulting in the warmest water, the most downwelling, and the highest heat flux anomalies, occurring slightly south of the eddy center. This would explain the off-center LHF and SHF peaks.

Most of the eddies identified are surface-intensified, however, subsurface-intensified eddies could lead to opposite SST anomalies and would likely impact turbulent heat fluxes in a different way. This study focuses on surface-intensified eddies. Recall from Section 2.1 that surface-intensified eddies will have a doming of the isopycnals for cyclones, resulting in negative SST and SLA anomalies. Anticyclones have a depression of the isopycnals, resulting in positive SST and SLA anomalies. The larger the eddy amplitude, the stronger the isopycnal deformation (e.g., Holte et al., 2013). And as we discovered from Figure 6, larger eddy amplitude corresponds to large heat flux anomalies. Within the Villas Bôas et al. (2015) paper, they did not separate surface-intensified from subsurface-intensified eddies and instead set this aside for future work. Distinguishing the two from surface observations is discuss very challenging (Assassi et al., 2016).
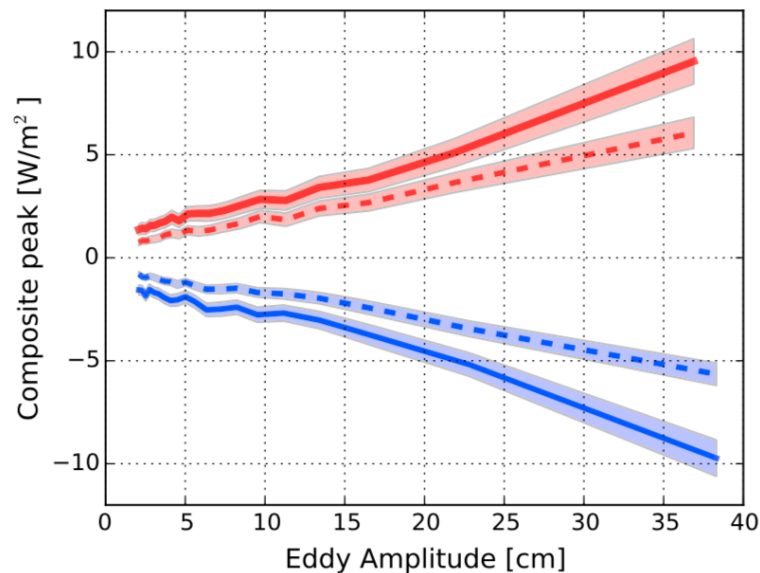

Figure 6: Plot of surface turbulent heat flux anomalies within eddies as a function of the respective eddy amplitude. Solid lines are LHF and dashed lines are SHF. Red lines are anticyclonic eddies and they are the maximum heat flux anomalies. Blue lines are cyclonic eddies and they show the minimum heat flux anomalies. The shadows around the lines are the confidence interval at one standard error of the mean. The anomalies here were computed from the averaged composite maps.

Eddy-induced LHF and SHF anomalies appear to differ depending on location. On average, eddy-induced turbulent heat flux anomalies are weak and not statistically significant over the South Atlantic. But in the BMC and AGR regions, the eddy-induced turbulent heat flux anomalies are significant. They can reach up to ~10 – 20 W/m² , which is the same order of magnitude as the amplitude of the large-scale annual cycle. It is unknown why eddy imprints are stronger in eddy-rich regions than "calmer" regions. More recent papers have also observed locational differences. In Leyba et al. (2017), an eddy near ocean fronts compared to one in a homogenous ocean had different impacts on heat flux anomalies. Hausmann and Czaja (2012) also show that anomalies associated with mesoscale eddies are stronger in energetic regions,

characterized by high SLA variability. We know that high SLA variability is associated with large-amplitude eddies (Chelton et al. 2011), so Villas Bôas et al. (2015) chooses to explore the relationship between LHF and SHF anomalies on eddy amplitudes.

Utilizing the averaged composite maps, they find the maximum absolute value of the anomalies to create Figure 6. Figure 6 confirms that larger eddy amplitude results in larger magnitude of heat flux anomalies. This is true regardless of eddy polarity, though the heat flux anomalies are negative for cyclonic eddies and positive for anticyclonic eddies. The order of magnitude is similar for both anticyclonic and cyclonic eddies.

5. Summary

The Villas Bôas et al. (2015) paper further confirmed that the ocean and atmosphere are coupled at the mesoscale by using ten years of satellite altimetry and remote sensed heat flux estimations. Satellite altimetry data was used alongside methodology produced by Chaigneau et al. (2008, 2009) to detect and track eddies. Heat flux estimates at a resolution of 0.25º x 0.25º were obtained from IFREMER. Villas Bôas et al. (2015) filtered heat flux data in time and space with a Hann window. The results revealed turbulent heat flux anomalies associated with eddies, such that anticyclonic eddies had positive anomalies and cyclonic eddies had negative anomalies.

The extent of the heat flux anomalies differed depending on the region of the eddy, such that eddy-rich regions such as the BMC and AGR had statistically significant heat flux anomalies (up to ~10-20 W/m^2). Meanwhile, quiescent regions were not statistically significant. The cause of the regional difference is unknown and requires further study. It is possible that LHF and SHF anomalies are stronger in regions of eddy genesis, but this is still only a hypothesis (Villas Bôas et al. (2015).

This study confirmed that heat flux anomalies have a positive correlation with anticyclonic eddies and a negative correlation with cyclonic eddies. It also confirmed that LHF and SHF anomalies are correlated to eddy amplitudes. The composite maps produced by this study revealed that the maximum/minimum heat flux anomaly is slightly off the eddy center. It shifts poleward for anticyclonic and equatorward for cyclonic. The β effect is likely the cause.

The turbulent heat flux anomalies associated with mesoscale eddies are significant. The intensity of these anomalies could have impacts beyond the atmospheric boundary layer, having potential effects on the large-scale atmospheric circulation. Their contribution to air-sea interaction should not be ignored, particularly in ocean-atmosphere coupled models.

References

Assassi, C., Morel, Y., Vandermeirsch, F., Chaigneau, A., Pegliasco, C., Morrow, R., Colas, F., Fleury, S., Carton, X., Klein, P., and Cambra, R. (2016), An Index to Distinguish Surface- and Subsurface- Intensified Vortices from Surface Observations, *J. Phys. Oceanogr.*, 46(8), 2529-2552.

Bakun, A. (2006), Fronts and eddies as key structures in the habitat of marine fish larvae: opportunity, adaptive response and competitive advantage, *Scientia Marina*., 70(2), 105-122.

Bentamy, A., K. B. Katsaros, A. M. Mestas-Nuñez, W. M. Drennan, E. B. Forde, and H. Roquet (2003), Satellite estimates of wind speed and latent heat flux over the global oceans, J. Clim., 16, 637–656, doi:10.1175/ 1520-0442(2003)016<0637:SEOWSA>2.0.CO;2.

Bentamy, A., Grodsky, S.A., Katsaros, K., Mestas-Nunez, A.M., Blanke, B., and Desbiolles, F. (2013), Improvement in airsea flux estimates derived from satellite observations, *Int. J. of Remote Sensing.*, 34(14), 5243-5261.

Cayan, D. R. (1992), Latent and sensible heat flux anomalies over the northern oceans: Driving the sea surface temperature, *J. Phys. Oceanogr.*, *22*(8), 859–881.

Chaigneau, A., A. Gizolme, and C. Grados (2008), Mesoscale eddies off Peru in altimeter records: Identification algorithms and eddy spatio-temporal patterns, *Prog. Oceanogr.*, *79*(2–4), 106–119, doi:10.1016/j.pocean.2008.10.013.

Chaigneau, A., G. Eldin, and B. Dewitte (2009), Eddy activity in the four major upwelling systems from satellite altimetry (1992–2007), *Prog. Oceanogr.*, *83*(1–4), 117–123, doi:10.1016/j.pocean.2009.07.012.

Chelton, D. B., M. G. Schlax, and R. M. Samelson (2011), Global observations of nonlinear mesoscale eddies, *Prog. Oceanogr.*, *91*, 167–216.

Chelton, D. B., and S.-P. Xie (2010), Coupled ocean-atmosphere interaction at oceanic mesoscales, *Oceanography*, *23*(4), 52–69.

Fairall, C., E. F. Bradley, J. Hare, A. Grachev, and J. Edson (2003), Bulk parameterization of air-sea fluxes: Updates and verification for the COARE algorithm, *J. Clim.*, *16*(4), 571–591.

Firing, E., and R. C. Beardsley (1976), The behavior of a barotropic eddy on a β-plane, *J. Phys. Oceanogr.*, *6*(1), 57–65.

Grodsky S. A., A. Bentamy, J. A. Carton, R. T. Pinker, 2009: Intraseasonal Latent Heat Flux Based on Satellite Observations. *Journal of Climate*, 22(17), 4539-4556. http://dx.doi.org/10.1175/2009JCLI2901.1

Hausmann, U., and A. Czaja (2012), The observed signature of mesoscale eddies in sea surface temperature and the associated heat transport, *Deep Sea Res., Part I*, *70*, 60–72.

Leyba, I.M., Saraceno, M. & Solman, S.A. Air-sea heat fluxes associated to mesoscale eddies in the Southwestern Atlantic Ocean and their dependence on different regional conditions. *Clim Dyn* **49,** 2491–2501 (2017). https://doi.org/10.1007/s00382-016-3460-5

Reynolds, R. W., T. M. Smith, C. Liu, D. B. Chelton, K. S. Casey, and M. G. Schlax (2007), Daily high-resolution-blended analyses for sea surface temperature, J. Clim., 20, 5473–5496, doi:10.1175/ 2007JCLI1824.1.

Santorelli, A., R. Pinker, A. Bentamy, K. Katsaros, W. Drennan, A. Mestas-Nuñez, and J. Carton (2011), Differences between two estimates of air-sea turbulent heat fluxes over the Atlantic Ocean, *J. Geophys. Res.*, *116*, C09028, doi:10.1029/2010JC006927.

Schultz, J., P. Schlussel, and H. Grassl, 1993: Water vapour in the atmosphere boundary layer over oceans from SSM/I measurements. *Int. J. Remote. Sensing*, 14, 2773-2789.

Villas Bôas, A. B., O. T. Sato, A. Chaigneau, and G. P. Castelão (2015), The signature of mesoscale eddies on the air-sea turbulent heat fluxes in the South Atlantic Ocean, *Geo- phys. Res. Lett.*, *42*, 1856–1862, doi:10.1002/2015GL063105.

Wunsch, C. (1999), Where do ocean eddy heat fluxes matter?, *J. Geophys. Res.*, *104*(C6), 13,235–13,249.